The Rac1 homolog CED-10 is a component of the MES-1/SRC-1 pathway for asymmetric division of the *C. elegans* EMS blastomere

Helen Lamb, Małgorzata Liro, Krista Myles, McKenzi Fernholz, Holly Anderson, and Lesilee S. Rose*

Department of Molecular and Cellular Biology, University of California, Davis

One Shields Ave., Davis, CA 95616

*Author for correspondence: lsrose@ucdavis.edu

Abstract

Asymmetric cell division is essential for the creation of cell types with different identities and functions. The EMS blastomere of the four-cell *Caenorhabditis elegans* embryo undergoes an asymmetric division in response to partially redundant signaling pathways. One pathway involves a Wnt signal emanating from the neighboring P2 cell, while the other pathway is defined by the receptor-like MES-1 protein localized at the EMS/P2 cell contact, and the cytoplasmic kinase SRC-1. In response to these pathways, the EMS nuclear-centrosome complex rotates so that the spindle forms on the anterior-posterior axis; after division, the daughter cell contacting P2 becomes the endodermal precursor cell. Here we identify the Rac1 homolog, CED-10, as a new component of the MES-1/SRC-1 pathway. Loss of CED-10 affects both spindle positioning and endoderm specification. Although MES-1 is still present at the EMS/P2 contact in *ced-10* embryos, SRC-1 dependent phosphorylation is reduced. These and other results suggest that CED-10 acts downstream of MES-1 and upstream of, or at the level of, SRC-1 activity. In addition, we find that the branched actin regulator ARX-2 is enriched at the EMS/P2 cell contact site, in a CED-10 dependent manner. Loss of ARX-2 results in spindle positioning defects, suggesting that CED-10 acts through branched actin to promote the asymmetric division of the EMS cell.

Introduction

Asymmetric cell division is the process by which dividing cells give rise to daughter cells with different identities and fates. This type of division occurs in all multicellular organisms and is necessary for cell type diversification during both embryonic development and adult tissue homeostasis (Inaba and Yamashita, 2012; Morin and Bellaiche, 2011; Venkei and Yamashita, 2018). A key aspect of asymmetric division is alignment of the mitotic spindle along a specific axis (Bergstralh and St Johnston, 2014; D'avino et al., 2005; di Pietro et al., 2016; Kotak, 2019; McNally, 2013). In many metazoan cell divisions requiring an oriented spindle, the microtubule pulling forces necessary to move the spindle are generated by the asymmetric localization of a conserved cortical complex. This force-generating complex contains the minus-end directed motor dynein, its partner dynactin, and the adaptor protein NuMA (LIN-5 in *C. elegans*, Mud in *Drosophila*). The complex can be recruited to the membrane or cortex by various adaptor and anchor proteins, and several different polarized cues have been identified that instruct spindle orientation (di Pietro et al., 2016; McNally, 2013; Morin and Bellaiche, 2011). For example, in many types of metazoan asymmetric divisions, the evolutionary conserved PAR proteins establish the polarity axis and influence the localization or activity of NuMA (LIN-5) and the force-generating complex. Wnt signaling pathways also act via NuMA (LIN-5) and dynein to align mitotic spindles with tissue polarity in several systems. However, for many cell types, the detailed mechanisms by which spindles are oriented remain to be elucidated (di Pietro et al., 2016; Gillies and Cabernard, 2011; Kotak, 2019).

The early *Caenorhabditis elegans* embryo serves as an excellent model for studying the molecular mechanisms of asymmetric division in different developmental contexts, as the embryo exhibits an invariant division pattern that includes multiple asymmetric divisions regulated by different cues (Griffin, 2015b; Pacquelet, 2017; Rose and Gonczy, 2014a). After fertilization, the zygote (or P0 cell) establishes molecular asymmetries that define the anterior and posterior embryonic poles. Following pronuclear meeting, the newly formed mitotic spindle rotates to align with the anterior-posterior axis and thus division creates an anterior somatic cell, AB, and a posterior germ-cell precursor, P1. The AB daughter divides symmetrically to give rise to ABa and ABp at the anterior and dorsal aspects of the embryo, respectively. The P1 cell divides asymmetrically to give rise to the EMS and P2 cells at the ventral and posterior aspects

61 of the embryo, respectively. EMS and P2 both divide asymmetrically again (Fig. 1A)(Griffin,
62 2015a; Pacquelet, 2017; Rose and Gonczy, 2014b).

63 The asymmetric division of the P0 cell is instructed by PAR polarity. In these cells, PAR
64 proteins antagonize one another's cortical localization to form mutually exclusive anterior and
65 posterior domains (Griffin, 2015b; Pacquelet, 2017; Rose and Gonczy, 2014a). In response to the
66 formation of the PAR domains, a cytoplasmic gradient of cell fate determinants forms along the
67 anterior-posterior axis. Downstream of PAR polarity cues, the force-generating complex
68 described previously localizes asymmetrically on the cortex and exerts microtubule pulling
69 forces that cause the nuclear-centrosome complex to rotate, such that the spindle forms along the
70 axis of PAR asymmetry (Kotak, 2019; Pacquelet, 2017; Rose and Gonczy, 2014a). The resulting
71 mitotic division gives rise to daughters that have inherited different quantities of PAR proteins
72 and cytoplasmic fate determinants and therefore proceed to adopt different fates. In the
73 asymmetric divisions of the posterior P1 daughter, mutually exclusive cortical PAR domains
74 form and the nuclear-centrosome complex rotates onto the axis of PAR polarity. The
75 mechanisms regulating nuclear rotation and unequal division of P1 are thought to be similar to
76 those in the one-cell (Kotak, 2019; Pacquelet, 2017; Rose and Gonczy, 2014a).

77 In contrast, the asymmetry of the EMS division is generated by two partially redundant
78 signaling pathways that require contact with EMS's neighboring cell, P2: a well-described Wnt
79 pathway and a less understood MES-1/SRC-1 pathway, involving the transmembrane tyrosine
80 kinase-like receptor MES-1, the cytoplasmic tyrosine kinase SRC-1 (Fig. 1A; reviewed in
81 (Maduro, 2017; Sawa, 2012)). In response to these pathways, the mitotic spindle orients on the
82 anterior-posterior axis, which requires a rotation of the nuclear-centrosome complex from its
83 initial left-right orientation (Fig. 1A). The anterior daughter of this division, MS, becomes a
84 mesoderm progenitor, while the posterior daughter E, born adjacent to P2, becomes an endoderm
85 progenitor.

86 Double mutant analysis has been the standard method for assigning genes to one of the
87 partially redundant EMS asymmetric division pathways. Homozygous maternal loss of function
88 for MES-1, SRC-1, or any of several Wnt pathway members causes a low rate of late or failed
89 EMS spindle rotations (Bei et al., 2002; Rocheleau et al., 1997; Schlesinger et al., 1999; Thorpe
90 et al., 1997; Walston et al., 2004). However, when a *mes-1* or *src-1* mutation is combined with
91 mutation of a Wnt pathway component, the rate of spindle rotation failure increases to 90-100%.

92 In contrast, *mes-1;src-1* double mutants have the same low frequency of spindle rotation defects
93 as *mes-1* and *src-1* single mutants. The MES-1 protein is localized to the EMS/P2 cell contact,
94 apparently in both cells, as this localization requires cell-cell contact specifically between these
95 cells (Bei et al., 2002; Berkowitz and Strome, 2000). Further, MES-1 is required for activation of
96 SRC-1 at the EMS/P2 contact, based on the staining pattern of an antibody that detects SRC-1-
97 dependent tyrosine phosphorylation (Bei et al., 2002). Thus, MES-1 and SRC-1 are part of a
98 pathway that is functionally redundant with Wnt signaling in promoting EMS spindle
99 positioning. The two pathways may converge on the conserved force generating complex
100 described earlier. Loss of the dynein heavy chain (DHC-1), dynactin (DNC-1), or LIN-5 results
101 in stronger spindle orientation defects than single mutants in either the MES-1/SRC-1 or Wnt
102 pathways, suggesting that LIN-5 and dynein may act in both pathways (Liro and Rose, 2016;
103 Zhang et al., 2007).

104 The induction of the E cell to form endoderm also depends on both the Mes and Wnt
105 pathways. Endoderm fate specification requires the Wnt ligand (MOM-2 in *C. elegans*,
106 expressed in the P2 cell), the transmembrane Frizzled receptor (MOM-5), and other conserved
107 Wnt pathway components (Rocheleau et al., 1997; Schlesinger et al., 1999; Thorpe et al., 1997).
108 Activation of this pathway ultimately results in nuclear export of the LEF-1/TCF-7 ortholog
109 POP-1 in the E cell, which allows endoderm-specific gene expression in this cell (Maduro, 2017;
110 Sawa, 2012). While mutation in either MES-1 or SRC-1 does not result in endoderm defects,
111 mutation of either in combination with strong loss of function mutations in Wnt pathway
112 components results in increased numbers of embryos without endoderm, and loss of SRC-1 was
113 shown to enhance the POP-1 nuclear export defect of Wnt pathway mutants (Sugioka et al.,
114 2011; Sugioka and Sawa, 2010; Sumiyoshi et al., 2011).

115 A previous study found that CED-10, one of three *C. elegans* Rac proteins, is required for
116 spindle orientation in the ABar blastomere of the eight-cell embryo, which is a Wnt dependent
117 pathway (Cabello et al., 2010). Rac proteins, a conserved subclass of the Rho GTPase family, are
118 involved in cytoskeletal regulation across diverse developmental contexts and many organisms
119 (Boreaux et al., 2007; Bustelo et al., 2007; Duquette and Lamache-Vane, 2014; Hall, 2012). The
120 same *C. elegans* study reported that *ced-10* mutant embryos exhibited abnormal EMS spindle
121 positioning in the four-cell embryo (Cabello et al., 2010). However, this phenotype was not
122 characterized, nor was the relationship between CED-10 and the signaling pathways known to

123 promote EMS spindle positioning. Therefore, we set out to define the genetic and molecular role
124 CED-10 plays in this asymmetric division. Here we demonstrate that CED-10 works in parallel
125 with the Wnt pathway in the EMS cell, where it acts downstream of MES-1 and upstream or at
126 the level of SRC-1 for both spindle orientation and endoderm specification.
127
128
129 **Results**
130 **The Rac1 homolog CED-10 is a member of the MES-1/SRC-1 pathway for EMS spindle**
131 **positioning**

132 Previous work showed that embryos from mothers homozygous for a null allele of *ced-*
133 *10(t1875)*, hereafter referred to as *ced-10* mutant embryos, exhibited defects in the division of
134 the ABar cell of the eight-cell embryo; this same study reported that CED-10 is required for
135 spindle positioning in EMS, but no data were shown for this or earlier divisions (Cabello et al.,
136 2010). We recently reported that *ced-10* mutant embryos exhibit normal nuclear and spindle
137 positioning movements during the division of the one-cell embryo (Price et al., 2022). However,
138 normal EMS division also requires the successful completion of the P1 division to produce
139 properly fated P2 and EMS cells (Fig. 1A). Thus, here we first examined the P1 division in *ced-*
140 *10* mutant embryos before proceeding to characterize the role of CED-10 in the EMS division.
141 To facilitate scoring spindle positioning, we generated a strain with *ced-10(t1875)* in a
142 GFP::tubulin background and compared embryos from this strain to control GFP::tubulin
143 embryos.
144 In control embryos, the P1 nuclear-centrosome complex rotated onto the anterior-
145 posterior axis prior to nuclear envelope breakdown (NEB) in all embryos (Fig. 1B). In
146 comparison, 21% of *ced-10*; GFP::tubulin embryos had a late or failed P1 spindle rotation (n=23,
147 Fig. 1B). PAR polarity is required for spindle orientation and for the identity of P1's daughter
148 cells, and so we next observed the localization of endogenously tagged mCherry::PAR-2
149 (mCh::PAR-2) in a *ced-10* strain also expressing GFP::tubulin. Late and failed P1 nuclear
150 rotations were again seen for *ced-10* embryos in this background (Fig. 1C). Nonetheless, all
151 embryos formed normally oriented PAR-2 domains, and the P2 cell inherited PAR-2 around its
152 entirety in embryos with normal or late rotation (n=12, n=11 for control). A small proportion of
153 *ced-10* embryos also inherited some PAR-2 in the EMS cell (1/12), but this was also seen in the

control embryos (2/11). In *ced-10* embryos in which the P1 spindle oriented with normal or late timing, the EMS blastomere was larger than P2 and divided before P2, as in controls. Together these results suggest that CED-10 may have a subtle role in P1 nuclear rotation, but in the vast majority of embryos, the P1 cell divides asymmetrically.

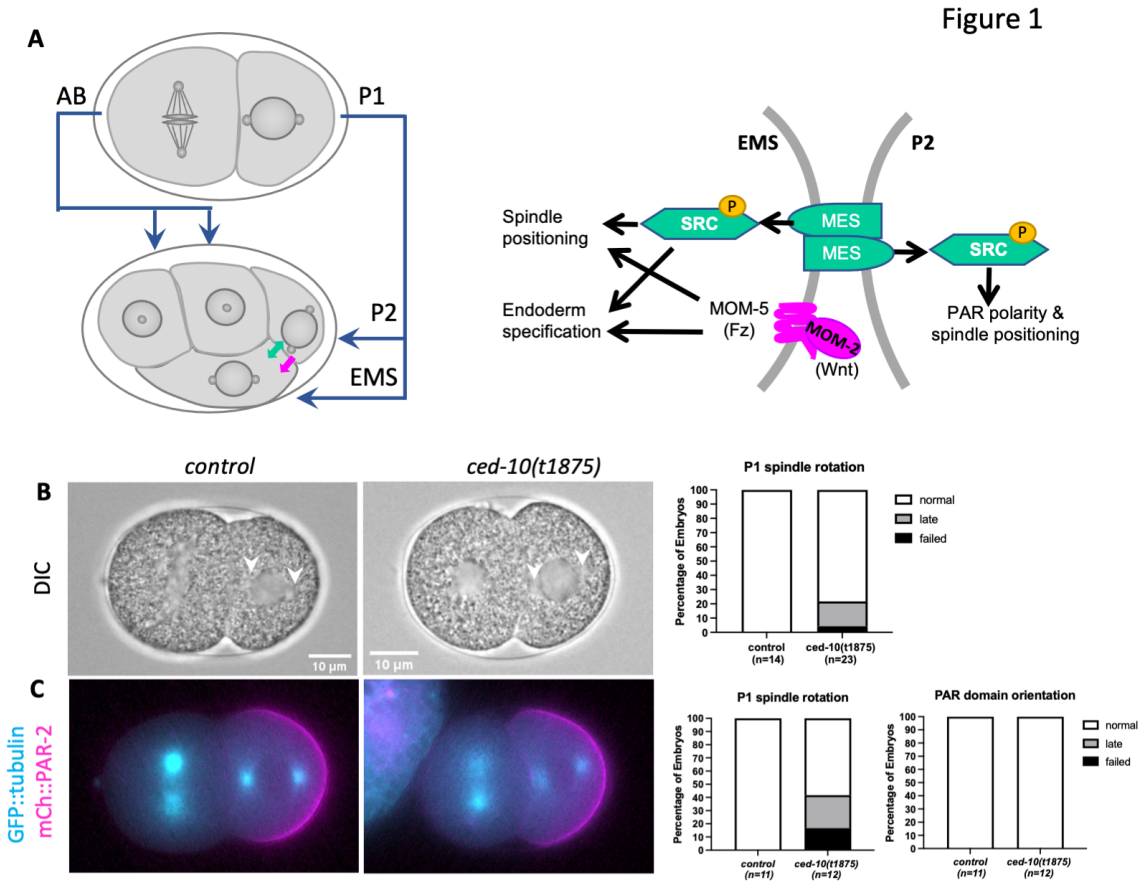

Figure 1. *ced-10* embryos undergo an asymmetric P1 division.
(A) Diagram illustrating the progression from two cells to four cells in the early *C. elegans* embryo. In this and all images, anterior is to the left and posterior to the right, ventral is top and dorsal is bottom. The asymmetric division of the P1 cell results in differentially fated EMS and P2 daughters. The EMS/P2 cell contact is enlarged at right, with key components of the MES-1/SRC-1 (green) and Wnt (magenta) signaling pathways labeled. (B) Representative control GFP::tubulin and *ced-10(t1875)*; GFP::tubulin embryos imaged by DIC during the second division, illustrating normal nuclear centrosome complex orientation on the anterior-posterior axis in P1. Arrows point to centrosomes. Graph shows quantification of normal, late or failed P1 nuclear rotation (see Methods). (C) Representative epifluorescence images of mCh::PAR-2 domains and GFP::tubulin in control and *ced-10(t1875)* embryos at the time of P1 nuclear rotation. Graphs show quantification of P1 nuclear rotation in this background and PAR-2 domain orientation.

174 We next examined the EMS division in *ced-10* embryos and observed that 43% of *ced-10*
175 embryos had a late or failed EMS spindle rotation (Fig. 2A, B). CED-10 appears to act in a Wnt-
176 dependent asymmetric division to orient the spindle of the ABar cell at the eight-cell stage
177 (Cabello et al., 2010). We therefore scored spindle positioning defects in *ced-10* mutants
178 depleted of MES-1, expecting that if CED-10 contributes to Wnt signaling for EMS spindle
179 positioning, *ced-10; mes-1(RNAi)* embryos would show a higher rate of complete failures of
180 EMS rotation. However, the proportion of failed and late rotations was not enhanced in *mes-*
181 *1(RNAi);ced-10* embryos compared to the single mutants. Instead, the combination of RNAi
182 depletion of MOM-2 (Wnt) and the *ced-10* mutant background increased the overall proportion
183 of abnormal EMS spindle positions to 77% and increased the rate of failed EMS spindle rotation
184 events to 53%, compared to 18% for *ced-10* alone (Fig. 2B). These results suggest that CED-10
185 plays a role in the MES-1/SRC-1 pathway for EMS spindle positioning.

Figure 2

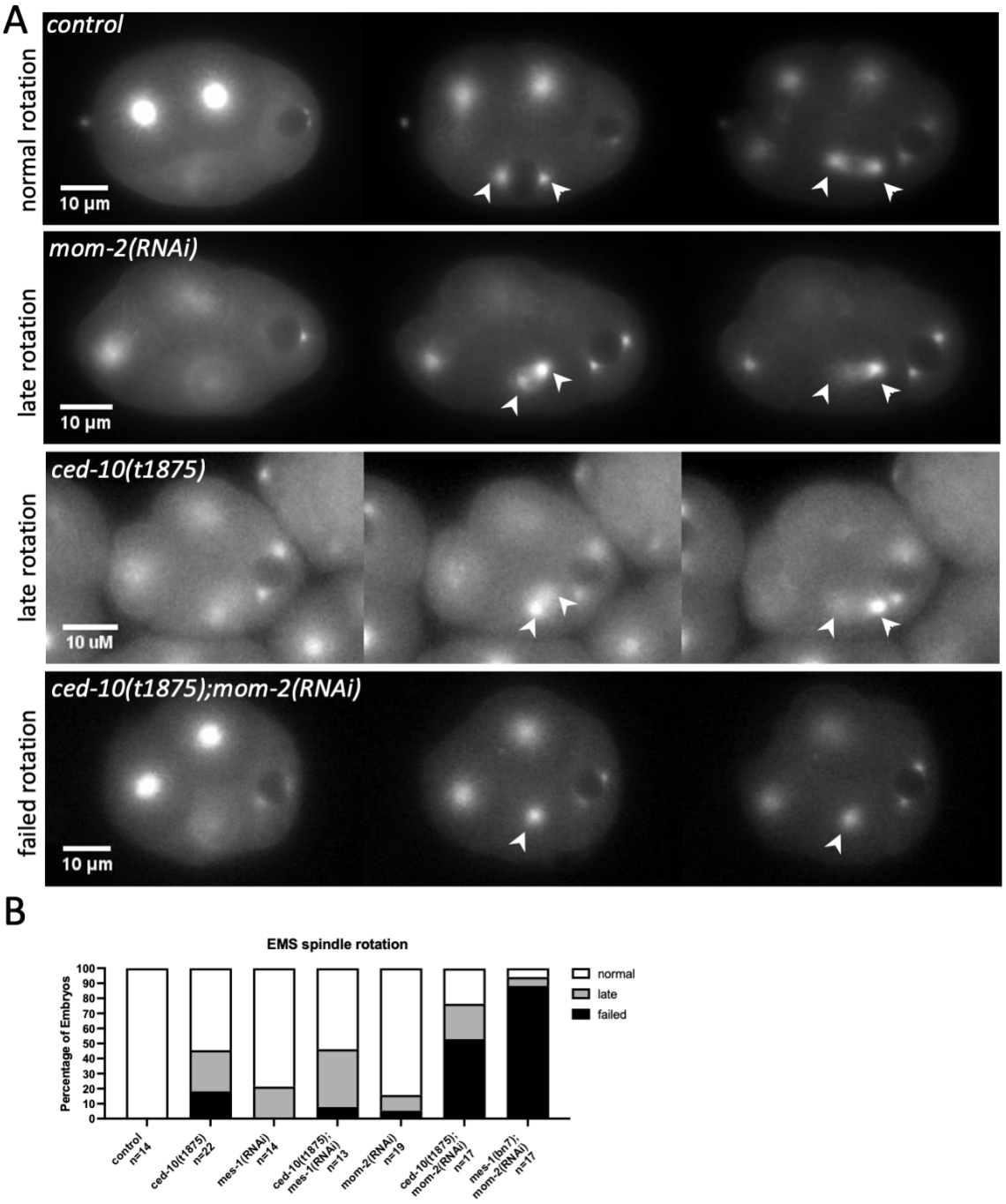

Figure 2. CED-10 acts in the MES-1/SRC-1 signaling pathway for EMS spindle positioning. (A) Representative stills from time-lapse images of GFP::tubulin embryos with the indicated genotypes, illustrating the three categories of EMS spindle orientation phenotypes observed. Arrowheads indicate EMS centrosomes. (B) Percentage of scored embryos for each indicated genotype with normal, late, or failed EMS rotation in a GFP::tubulin background. To ensure that the enhanced EMS defects were not indirectly caused by abnormal P1 division, only embryos with normal or late P1 spindle rotation were included in the analysis for *ced-10* and *ced-10; mom-2(RNAi)* embryos; 24% of *ced-10; mom-2(RNAi)* embryos had a late or failed P1 rotation, similar to that of *ced-10* alone.

195 **CED-10 is not required for spindle positioning in the P2 cell**
196

197 The MES-1 protein is localized exclusively to the EMS/P2 cell contact in wild-type
198 embryos (Berkowitz and Strome, 2000). The MES-1/SRC-1 signaling pathway, in addition to its
199 importance in EMS spindle positioning and endoderm fate specification, is required for orienting
200 PAR polarity and spindle positioning in the P2 cell (Fig. 1A)(Bei et al., 2002; Berkowitz and
201 Strome, 2000). At birth, P2 inherits the posterior PARs such as PAR-2 uniformly around the
202 cortex. Before division, a new PAR-2 domain forms, but in a different orientation to the previous
203 P lineage divisions: The "posterior" PARs disappear from the dorsal side of the cell, including
204 part of P2/ABp cell contact, such that they are present in a ventral "V" that includes the P2/EMS
205 cell contact (Fig. 3); the "anterior" PARs localize to the reciprocal dorsal side of the cell (Arata
206 et al., 2010; Rose and Gonczy, 2014a). The P2 spindle orients along this new axis of PAR
207 asymmetry. In *mes-1(RNAi)* or mutant embryos, reciprocal PAR polarity domains form in the P2
208 cell but are misoriented in ~70% of embryos; specifically, PAR-2 disappears from the P2/EMS
209 as well as the P2/ABp cell contact in these embryos, resulting in a posterior PAR-2 domain. The
210 P2 spindle is oriented along this anterior-posterior axis in ~50% of *mes-1* mutant embryos, the
211 proportion being lower because spindle and polarity are uncoupled in some embryos; many
212 divisions are also equal in terms of daughter cell size (Arata et al., 2010).
213 If *ced-10* disrupts MES-1 function, then asymmetric division of the P2 cell should be
214 affected. We first examined the P2 division from the same GFP::tubulin movies used above.
215 Because the focal plane of these movies was optimized for scoring the EMS division, the final
216 orientation or equalness in the P2 division was not always visible. Thus, we scored the initial
217 orientation of the P2 nuclear-centrosome complex. The P2 nuclear-centrosome complex aligns
218 with the PAR polarity axis through either centrosome migration or partial nuclear rotation where
219 one centrosome becomes closely associated with P2/EMS cell contact (Arata et al., 2010;
220 Berkowitz and Strome, 2000); the nuclear-centrosome complex and the subsequent spindle are
221 thus oriented on a somewhat dorsal-ventral axis, approximately 45° relative to the anterior-
222 posterior axis (Fig. 3A). For simplicity, we refer to the close association of the centrosome with
223 the cell contact as "centrosome cueing". We found that in control GFP::tubulin embryos,
224 centrosome cueing occurred in all embryos, usually before EMS NEB (11/13; 2 embryos cued by
225 EMS NEB + 40sec). Centrosome cueing also occurred in 100% of *ced-10(t1875)* embryos,

226 within the same time range as controls (n=9) (Fig. 3A, B). In comparison, in the majority of *mes-*
227 *1(bn7)* embryos, the P2 nuclear-centrosome complex did not cue to the cell contact (13/14),
228 although in some embryos the centrosomes achieved a roughly dorsal-ventral orientation (Fig.
229 3A), as previously reported.

230 To further test for a *mes-1* like polarity phenotype, we examined P2 polarity in embryos
231 expressing mCh::PAR-2 and GFP::tubulin. In the majority of control embryos and *ced-10(t1875)*
232 mutant embryos, a PAR-2 domain formed on the ventral side of the cell as expected (Fig. 3B). In
233 one case for each, PAR-2 remained uniform, and in one case for each, PAR-2 disappeared from
234 the posterior of the P2 cell first. The latter is an opposite pattern to the defects noted above for
235 *mes-1* embryos. Thus, *ced-10* does not affect the orientation of the PAR-2 domain in the P2 cell.
236 In this data set, we again observed that in 100% of *ced-10* embryos (n = 10), the P2 nuclear-
237 centrosome complex cued to the P2/EMS cell contact, within the same time range as controls
238 cued (n =10). Together these data indicate that polarity and orientation of the P2 division are not
239 affected by loss of CED-10.

240 We also examined the localization of MES-1. Although endogenously tagged
241 mNeonGreen::3xFLAG::MES-1 is not visible in live embryos until the eight-cell stage (Heppert
242 et al., 2018), we found that anti-FLAG antibody staining showed the expected MES-1
243 localization at the EMS/P2 cell contact. MES-1 was also localized at the EMS/P2 contact in *ced-*
244 *10(RNAi*) embryos (Fig. 3C). The absolute intensity at the contact and in the cytoplasm were
245 lower in *ced-10* embryos compared to controls and thus CED-10 depletion may affect overall
246 MES-1 levels. Nonetheless, a higher cortical intensity of MES-1 at the EMS/P2 contact, relative
247 to the cytoplasm, was still present (Fig. 3C). These results indicate that CED-10 is not required
248 for MES-1 localization to the EMS/P2 contact per se. Together with the observations of a normal
249 P2 division in *ced-10* embryos, these results suggest that CED-10 does not affect MES-1 activity
250 and acts downstream of MES-1 in the pathway.

Figure 3

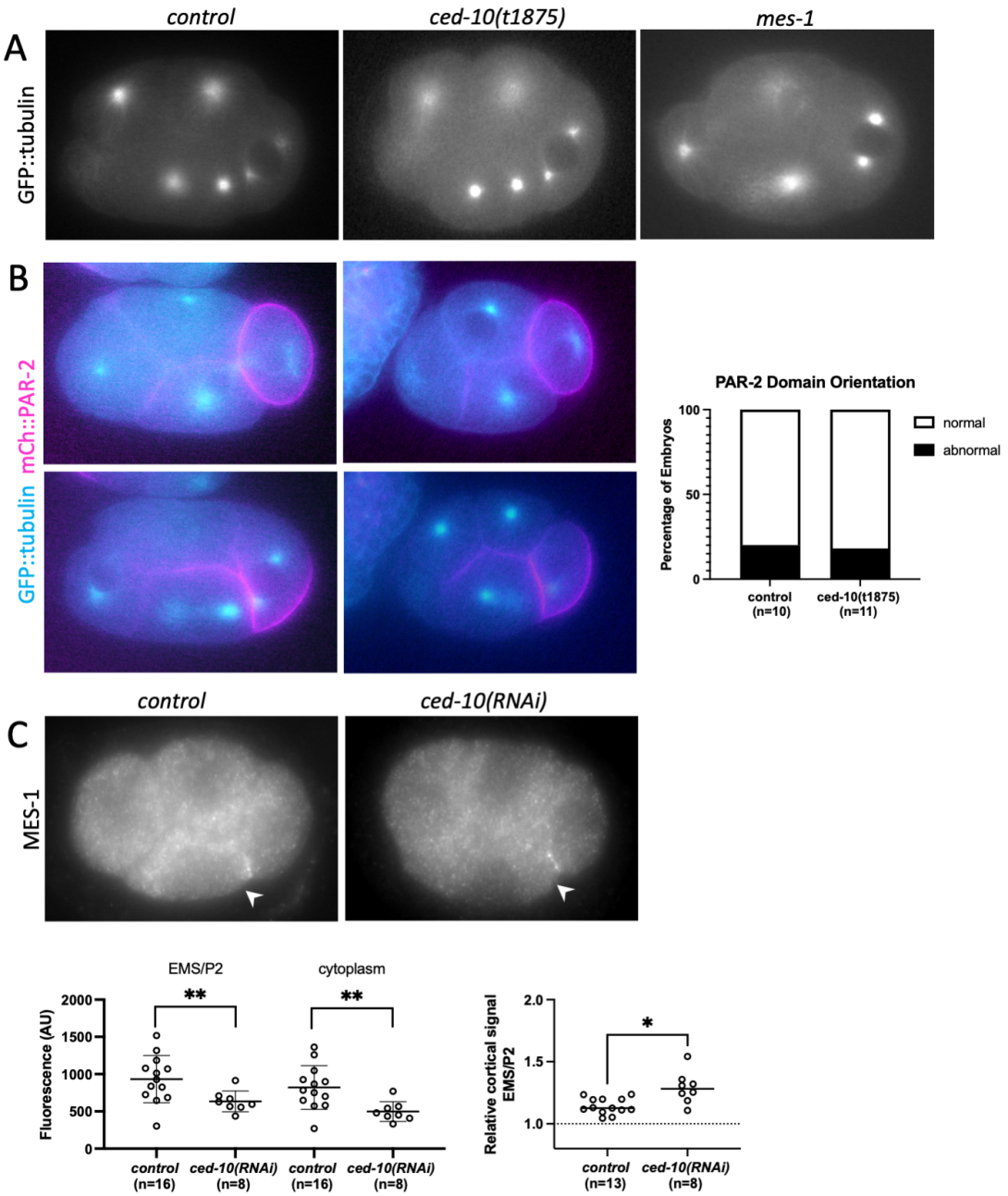

Figure 3. CED-10's role in MES-1/SRC-1 signaling is downstream of MES-1.
(A) Representative epifluorecence images of expressing GFP::tubulin embryos illustrating normal cueing of the P2 centrosome in control and *ced-10* embryos compared to *mes-1.* (B) Representative epifluorecence images of control and *ced-10* embryos expressing transgenic GFP::tubulin (cyan) and mCh::PAR-2 (magenta). Top panels show inheritance of PAR-2 around the entire periphery of P2; lower panels show formation of the PAR-2 domain. Graph shows percentage abnormal versus normal PAR-2 domains. (C) Epifluorescence microscopy of control and *ced-10(RNAi)* mNeonGreen::3xFLAG::MES-1 embryos immunostained for the FLAG epitope. Graphs below show quantification of absolute cortical and cytoplasmic intensities (left) and the cortical levels at the EMS/P2 contact relative to the cytoplasmic background (right).

262

263 **CED-10 is required for normal levels of SRC-1 dependent phosphotyrosine staining**

264

265 We next set out to determine whether CED-10 affects SRC-1. Staining of four-cell *C.*
266 *elegans* embryos with the Y99 antibody, which recognizes phosphotyrosine, results in an
267 enriched signal at the EMS/P2 contact compared to other contacts, which is SRC-1-dependent.
268 Further, *mes-1* mutants show a loss of the enrichment, but not cell contact staining, which
269 supports the model that MES-1 activates SRC-1 (Bei et al., 2002). However, whether SRC-1
270 protein itself is enriched at that EMS/P2 contact relative to other contacts in the four-cell embryo
271 has not been tested. We therefore examined the localization of SRC-1 using a strain with SRC-1
272 endogenously tagged with GFP (Zhu et al., 2020a; Zhu et al., 2020b). SRC-1::GFP was
273 cortically localized to all cell contacts at the four-cell stage, but was not enriched at the EMS/P2
274 contact compared to other cell contacts (Fig. 4A). These results together with prior findings
275 suggest that the asymmetric localization of SRC-1 kinase activity is caused by asymmetric
276 activation of SRC-1 at the EMS/P2 contact. The cortical localization of SRC-1::GFP was not
277 altered in *ced-10(RNAi)* embryos (Fig. 4A).
278 Four-cell embryos were also stained with the Y99 anti-phosphotyrosine antibody. While
279 Y99 staining was still enriched at the EMS/P2 contact compared to the EMS/ABp contact in
280 some *ced-10(t1875)* embryos, many embryos showed less enrichment than in wild-type (Fig.
281 4B). However, the average enrichment of the *ced-10* embryos was higher than for *mes-1*
282 embryos, which had no enrichment of Y99 signal at the EMS/P2 contact, as previously reported
283 (Bei et al., 2002).
284 In addition to EMS spindle positioning, MES-1 and SRC-1 are required for endoderm
285 fate specification in the E daughter cell in parallel with Wnt signaling. That is, although loss of
286 MES-1 or SRC-1 alone does not affect the formation of intestinal cells, loss of either enhances
287 the variable intestine-minus phenotypes of Wnt pathway mutants (Bei et al. 2002). Since our
288 results suggested that CED-10 affects SRC-1 activity at the EMS/P2 contact, we therefore asked
289 whether loss of CED-10 affects the formation of intestinal tissue in late-stage embryos. As seen
290 in prior studies (Bei et al., 2002; Rocheleau et al., 1997; Thorpe et al., 1997), we found that
291 *mom-2(RNAi)* embryos did not hatch but did form intestinal tissue as scored by the presence of
292 gut granules (Fig. 4C), while the majority of *mom-2(RNAi); mes-1(bn7)* embryos did not form

intestinal tissue. All *ced-10(t1875)* embryos had intestinal tissue, but a large proportion of *ced-10(t1875)*; *mom-2(RNAi)* embryos did not exhibit gut granules (Fig. 4C). These data indicate that CED-10 is required for proper specification of endoderm tissue in parallel with Wnt signaling. Together with the results of anti-phosphotyrosine staining, this observation suggests that CED-10 acts upstream of both EMS spindle positioning and endoderm fate specification by promoting enhanced SRC-1 activity or the accumulation of SRC targets at the EMS/P2 contact.

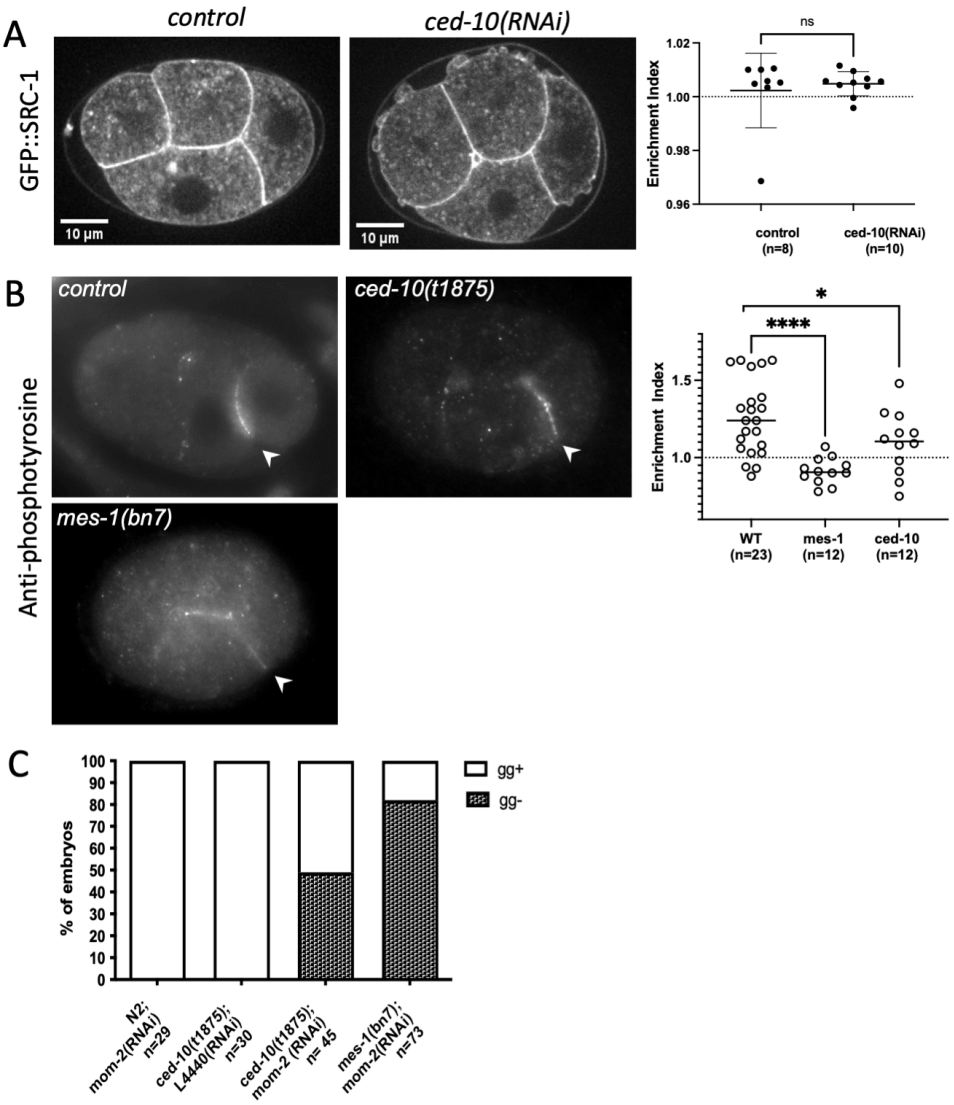

Figure 4. CED-10 is required for endoderm specification in parallel to Wnt signaling
(A) Representative confocal fluorescence images of GFP::SRC-1 in control and *ced-10(RNAi)* embryos. Graph shows the "enrichment index", the level at the EMS/P2 contact compared to the level at the EMS/ABp contact. (B) Representative epifluorecence images of embryos stained for SRC-1-dependent phosphotyrosine in the indicated genotypes. Graph shows the "enrichment index" as for (A). (C) Proportion of embryos with and without gut granules in the indicated genotypes.

306 **CED-10 and ARX-2 are localized at cell contacts at the four-cell stage**

307

308 To gain further insight into the function of CED-10 in MES-1/SRC-1 signaling, we
309 characterized the localization of GFP::CED-10 in four-cell embryos, using an integrated
310 GFP::CED-10 transgene under transcriptional control by the *ced-10* promoter (Ziel et al., 2009).
311 This transgene was previously shown to rescue the defects of *ced-10 (n1993),* which is a viable
312 allele of *ced-10* (Lundquist et al., 2001). We crossed this transgene into the *ced-10* null
313 background and found that GFP::CED-10; *ced-10(t1875)* embryos appeared less round than *ced-*
314 *10* mull embryos, and embryonic lethality was sufficiently rescued to maintain the strain
315 homozygous for *ced-10*. In early embryos, GFP::CED-10 was present on all cell-cell contacts
316 including at the four-cell stage (Fig. 5A). The cell contact signal and the cytoplasmic signal were
317 both reduced to background levels by RNAi of *ced-10.* Although *GFP::CED-10; ced-10(t1875)*
318 embryos exhibited many small cortical protrusions throughout the first few mitotic divisions,
319 similar to *ced-10(t1875)* embryos (Price et al., 2022), *GFP::CED-10; ced-10(t1875)* embryos did
320 not exhibit EMS division orientation defects. In addition, *GFP::CED-10; ced-10(t1875); mom-*
321 *2(RNAi)* embryos did not show the higher rate of defective spindle orientations observed for *ced-*
322 *10(t1875); mom-2(RNAi)* embryos examined in parallel (Fig. 5B). These results indicate that
323 GFP::CED-10 is functional in the early embryo for EMS spindle positioning. Quantification of
324 the relative cortical intensity of GFP::CED-10 at the EMS/P2 contact revealed a very slight
325 enrichment compared to the EMS/ABp contact on average (Fig. 5C). The GFP::CED-10
326 localization pattern is consistent with a cortex-localized mechanism of action for CED-10 in
327 EMS.

328 Rac proteins can signal through the WAVE complex or WASp proteins, which both
329 activate the Arp2/3 complex to nucleate branched actin (Saenz-Narciso et al., 2016; Shakir et al.,
330 2008). Therefore, we hypothesized that CED-10 contributes to EMS asymmetric division by
331 promoting branched actin at the EMS-P2 contact. Although prior studies have shown that
332 branched actin reporters localize to the cell surface at the one-cell stage and to cell-cell contacts
333 during ventral enclosure (Chan et al., 2018; Sawa et al., 2003), the localization of branched actin
334 at the four-cell stage has not been reported. We visualized ARX-2, the Arp2 member of the
335 Arp2/3 branched actin nucleating complex, with an integrated ARX-2::GFP fusion transgene
336 under transcriptional control by the *arx*-2 promoter (Sarov et al., 2012). Consistent with our

hypothesis, ARX-2::GFP was present at all cortical surfaces of the embryo and was also enriched at the EMS/P2 contact relative to the EMS/ABp contacts (Fig. 5D). Furthermore, the cortical localization of ARX-2::GFP at the EMS/P2 contact was decreased with *ced-10(RNAi)*, suggesting that CED-10 increases the levels of branched actin at the EMS/P2 cell-cell contact (Fig. 5D).

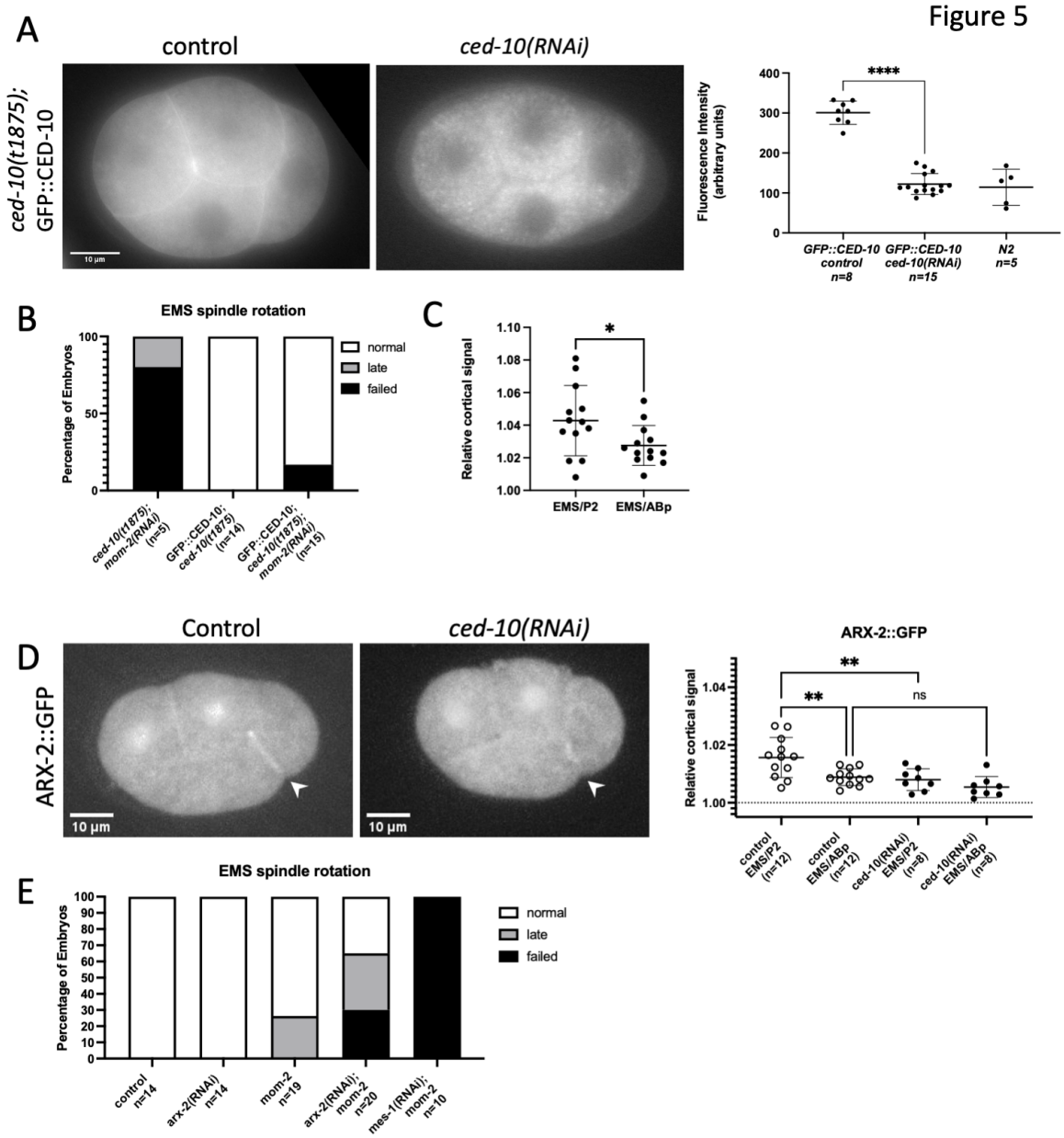

Figure 5. GFP::CED-10 and ARX-2::GFP are cortically localized in four-cell embryos
A) Representative wide-field fluorescence image of GFP::CED-10 in embryos treated with control RNAi (empty L4440 vector) or *ced-10* RNAi. Graph at right shows quantification of total background-corrected embryonic fluorescence intensity of GFP::CED-10 rescue embryos with and without *ced-10(RNAi)*. (B) Percentage of scored embryos with normal, late, and failed EMS spindle rotations for the indicated

genotypes. (C) Quantification of relative cortical CED-10::GFP fluorescence intensity, normalized to cytoplasm, at both the EMS/P2 and EMS/ABp contacts. (D) Representative maximum Z projections from confocal fluorescence microscopy of ARX-2::GFP in control and *ced-10(RNAi)* embryos. Graph shows relative cortical ARX-2::GFP fluorescence intensity, normalized to cytoplasm, at both the EMS/P2 and EMS/ABp contacts in the indicated genotypes. (E) Percentage of scored embryos with normal, late, and failed EMS spindle rotations for the indicated genotypes.

ARX-2 is required for EMS spindle positioning

To test whether ARX-2 and thus branched actin contributes to EMS spindle positioning, we first depleted ARX-2 by RNAi in GFP::tubulin; *mom-5(zu193)* (*Frizzled* null) embryos, one of the standard Wnt mutant backgrounds used in studies of EMS spindle positioning (Cabello et al., 2010; Liro and Rose, 2016). Unexpectedly, we found that *mom-5(zu193); arx-2(RNAi)* embryos displayed a high rate of P1 spindle rotation defects, with 56% completely failed rotations, compared to 8% for *mom-5(zu193)* and 7% for *arx-2(RNAi)* GFP::tubulin embryos. EMS spindle positioning was then scored in only the embryos with a normal or late rotation, which would allow for normal fating of the EMS and P2 blastomeres. In this subset, depletion of ARX-2 in a *mom-5(zu193)* background appeared to enhance the rate of defective spindle rotations observed in *mom-5* alone (Fig. S1); however, given the small sample size it is difficult to conclude from these data whether ARX-2 is required for EMS spindle positioning.

MOM-5/Frizzled was recently shown to affect pulling forces in the one-cell embryo, independent of its role in Wnt signaling (Sugioka et al., 2017). Thus, we repeated RNAi of ARX-2 in embryos from *mom-2(or42)* (Wnt) mothers. In these experiments, we did not observe P1 spindle rotation defects for either *mom-2* embryos or *mom-2; arx-2(RNAi)* embryos; however, ARX-2 RNAi enhanced the EMS spindle positioning defects of *mom-2* embryos (Fig. 5E). Together these results show that ARX-2 is required for spindle positioning in the EMS cell in a pathway parallel to the Wnt pathway, consistent with ARX-2 and branched actin acting downstream of CED-10 to promote spindle positioning in the MES-1/SRC-1 pathway. Given the observation of P1 defects in *arx-2(RNAi); mom-5* embryos, as well as P1 defects in some *ced-10* embryos as noted earlier, we also examined *ced-10* RNAi in the *mom-5*; GFP::tubulin background. We observed a complete failure of P1 rotation in 40% of *ced-10(RNAi); mom-5* embryos, an increase compared to *mom-5* alone (Fig. S1). However, *ced-10(t1875); mom-*

381 *2(RNAi)* did not exhibit an increased proportion of completely failed or late P1 spindle rotations
382 (Fig.S1). These results suggest the P1 failure phenotype is due to an interaction between the
383 Frizzled ortholog MOM-5 and the branched actin cytoskeleton.
384

Supplemental Fig. 1

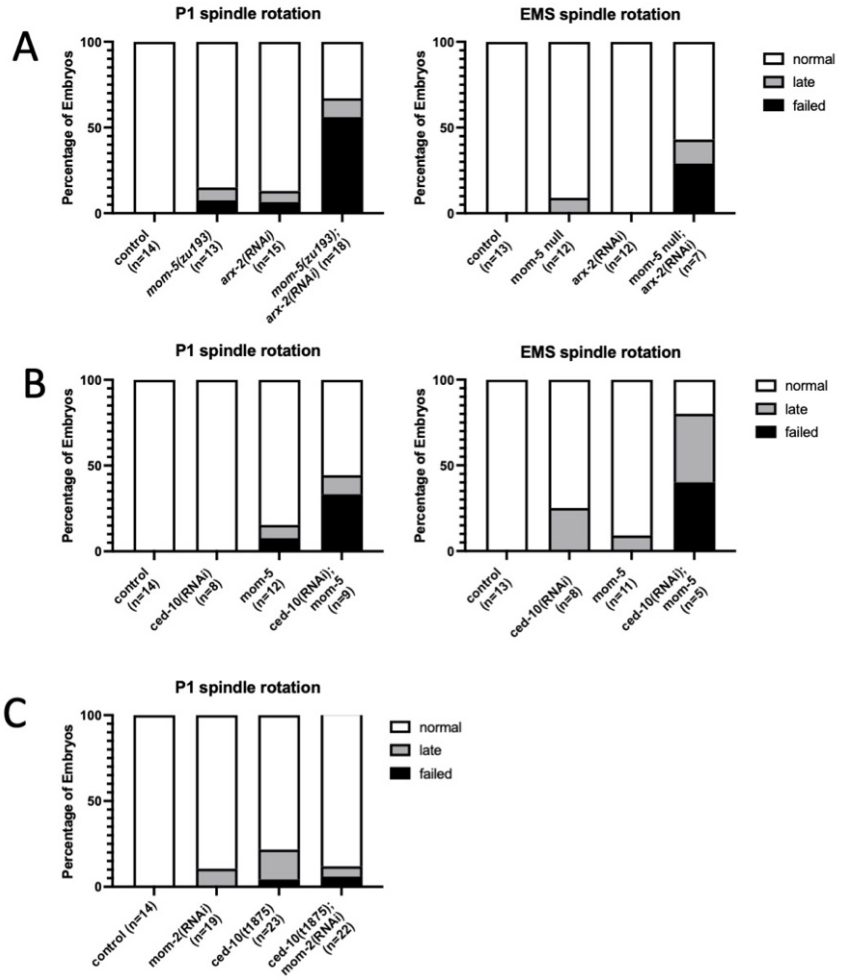

385

386 **Figure S1. ARX-2 and CED-10 genetically interact with MOM-5(Frizzled) during P1 nuclear**
387 **rotation.** Percentage of scored embryos with normal, late, and failed EMS spindle rotations for the
388 indicated genotypes. (A) Examination of P1 and EMS nuclear rotation in *arx-2; mom-5* double mutants.
389 (B) P1 and EMS nuclear rotation in *ced-10; mom-5* double mutants. (C) P1 rotation in *ced-10; mom-2*
390 double mutants.
391

392

393

394 **Discussion**

395

396 In this study, we demonstrate that the *C. elegans* Rac protein CED-10 plays an important
397 role in the asymmetric division of the EMS cell of the early embryo, which is regulated by
398 partially redundant Wnt and MES-1/SRC-1 signaling pathways. Our data are consistent with
399 CED-10 being a novel member of the MES-1/SRC-1 pathway. Our genetic and localization
400 analyses suggest that CED-10 acts downstream of MES-1 and upstream or at the level of SRC-1.
401 First, MES-1 was still present at the P2/EMS contact site, and *ced-10* embryos did not exhibit the
402 defects in PAR-2 polarity and spindle orientation that are known to result from loss of MES-1.
403 Thus, although we cannot rule out a redundant role in the P2 division, CED-10 does not appear
404 to be essential for MES-1 activity. At the same time, *ced-10* embryos did show reduced
405 enrichment of SRC-dependent phospho-tyrosine signal at the EMS/P2 contact. The antibody
406 used for this immunostaining experiment recognizes phosphorylated tyrosine and is a readout for
407 both SRC-1 autophosphorylation and phosphorylation of its targets (Bei et al., 2002); thus loss of
408 CED-10 could affect the activation of either SRC-1 or its targets. A GFP-tagged version of SRC-
409 1 was present at cell-cell contacts, but was not enriched at the EMS/P2 contact, nor was SRC-1
410 localization altered by *ced-10(RNAi)*. These data argue against a role in the asymmetric
411 recruitment of SRC-1 itself to the EMS/P2 cell contact. Instead, we propose that CED-10
412 promotes the cortical recruitment or retention of active SRC-1 or its targets at the EMS/P2
413 contact. A detailed analysis of this role will require future work uncovering direct targets of
414 SRC-1 in EMS, since only one target in the early embryo has thus far been proposed (Sumiyoshi
415 et al., 2011).

416 Our studies also reveal that ARX-2 and thus branched actin are required for the
417 asymmetric division of the EMS cell. The defects in spindle positioning in *arx-2(RNAi)* embryos
418 were very similar to those exhibited by *ced-10* embryos, and ARX-2::GFP was present at higher
419 levels at the EMS/P2 cell contact compared to other contacts in a manner dependent on CED-10.
420 Thus CED-10 appears to act through the generation of branched actin to promote spindle
421 positioning in the EMS cell. Interestingly, these experiments also uncovered an apparent genetic
422 interaction between branched actin and the Frizzled ortholog MOM-5 at the two-cell stage. In the
423 absence of MOM-5, branched actin depletion with RNAi against *arx-2* or *ced-10* caused a high
424 rate of failed P1 spindle rotations. Previous work implicated the Frizzled/MOM-5 protein and the

425 adenomatous polyposis coli (APC) homolog APR-1 in the regulation of microtubule dynamics
426 during mitotic spindle positioning of the one-cell *C. elegans* embryo. This mechanism is
427 dependent on PAR polarity but independent of the MOM-2 ligand (Sugioka et al., 2017; Sugioka
428 et al., 2011). As the P1 cell divides asymmetrically in a PAR dependent manner, it is possible
429 that Frizzled and APR-1 participate in a similar mechanism of regulating microtubule dynamics
430 for P1 spindle rotation as well. Based on the enhanced rate of P1 defects in *arx-2; mom-5* double
431 mutants, branched actin is likely required in a parallel pathway for either spindle positioning or
432 PAR polarity. It has recently been shown that PAR polarity in the P1 cell is established through
433 redundant mechanisms, at least one of which involves the actomyosin skeleton (Koch and Rose,
434 2023; Ng et al., 2023).

435 Prior work characterized a role for Rac1/CED-10 in spindle positioning of the ABar cell
436 of the eight-cell *C. elegans* embryos (Cabello et al., 2010). Wnt signaling instructs the mitotic
437 spindle of ABar to set up at a perpendicular angle to the orientation of the three other AB cell
438 spindles. This ABar spindle orientation pathway, like the Wnt-dependent pathway for EMS
439 spindle positioning, is transcription-independent (Schlesinger et al., 1999; Walston et al., 2004).
440 In the ABar cell, Wnt signaling appears to be the predominant mechanism because mutations in
441 the Wnt components cause failure of spindle orientation with high penetrance. Further,
442 overexpression of CED-10 resulted in slight rescue of Wnt mutant spindle orientation defects,
443 and genetic analysis showed that CED-10 acts downstream of Wnt signaling for cell-corpse
444 clearance in the later embryo and distal tip cell migration in the larvae (Cabello et al., 2010). In
445 contrast, our analyses show that CED-10 is a new component of the MES-1/ SRC-1 pathway for
446 both endoderm specification and spindle positioning in the EMS cell, rather than part of the Wnt
447 pathway. SRC-1 has also been shown to contribute to ABar spindle positioning, but its precise
448 role is unknown, and MES-1 does not appear to be present in the AB cells. Together these
449 observations and our findings raise the possibility that SRC-1, CED-10 and ARX-2 work
450 together in the ABar cell to promote spindle position, but downstream of Wnt signaling.

451 The data presented on the role of CED-10 in the EMS division are very similar to those
452 reported previously for the PIG-1 kinase. PIG-1 is a PAR-1 related kinase that has partially
453 redundant roles with PAR-1 in the one-cell embryo. During the EMS division however, genetic
454 analyses placed PIG-1 in the MES-1/SRC-1 pathway while PAR-1 appears to act in the Wnt
455 pathway. Loss of PIG-1 resulted in defects in both endoderm specification and spindle

positioning, as seen here for loss of CED-10. Further studies are required to determine the mechanistic links among SRC-1, CED-10, ARX-2 and PIG-1 during this asymmetric division in *C. elegans*, and it will be interesting to learn if this mechanism is utilized by other cells in *C. elegans* or in other organisms.

Data availability

Data necessary for confirming the conclusions of this study are present within the manuscript text or figures; this research did not generate large data sets but raw data and images are available upon request. Strains are available upon request from the corresponding author or the CGC.

Acknowledgements

We thank members of the Rose and McNally labs for helpful discussions, and Daniel A. Starr, Bruce W. Draper, and Jennifer Heppert for experimental advice. We are grateful to Guangshuo Ou, Martha Soto, Karen Oegema, Francis McNally, and Erik Lundquist for strains and plasmids. Many strains were obtained from the *Caenorhabditis* Genetics Center, which is funded by the National Institutes of Health Office of Research Infrastructure Programs (P40 OD010440) for strains. The 3i Marianas spinning disk confocal and the Nikon laser scanning confocal used in this study were purchased using a National Institutes of Health Shared Instrumentation Grant [1S10RR024543-01]. We thank the MCB Light Microscopy Imaging Facility, which is a UC-Davis Campus Core Research Facility, for the use of this microscope. This work was funded by awards from the National Institutes of Health Grant[R01GM68744] and the National Institute of Food and Agriculture [CA-D*-MCB-6239-H] to LSR. Support for HL and ML was also provided by the UC Davis BMCDB Graduate Group and a National Institutes of Health training grant to HL [T32 GM 007377].

Materials and Methods

Strains

Nematodes were maintained on Modified Youngren's Only Bacto-Peptone (MYOB) agar plates, seeded with *E. coli* OP50 using standard procedures (Brenner, 1974; Church et al., 1995; Stiernagle, 2006). Temperature sensitive strains were maintained at 16°C and others were maintained at ambient temperature (22-24°C).

Table 1. Strains used

Strain number	Genotype	Source or reference
EU384	dpy-11(e1180) mom-2(or42) / nT1 [let-?(m435)] V	CGC
FM126	unc-119 (ed3); ruIs57 [pAZ147: pie-1/b-tubulin::GFP; unc-119 (+)]; itIs37 [unc-119(+) pie-1::mCherry::H2B]; him-8 (e1489) IV	(Cortes et al., 2015)
GE4047	ced-10(t1875) / nT1 [qIs51(pha::GFP)] IV; +/ nT1 V	(Cabello et al., 2010)
GOU3475	src-1(cas605[src-1::gfp]) I	(Zhu et al., 2020b)
LP527	mes-1(cp240[mes-1::mNG-C1^3xFlag]	(Heppert et al., 2018)
NK336	qyIs28 [ced-10p::GFP::ced-10; unc-119(+); unc-119(ed4)	CGC; (Lundquist et al., 2001)
RL262	mom-5(zu193) unc-13(e1091)/hT2 I; + /hT2 III; ruIs57[pie-1::GFP::tubulin unc-119(+)]	(Liro and Rose, 2016)
Rl263	ced-10(t1875) / nT1 [qIs51(pha::GFP)] IV; +/ nT1 V; ruIs57[pie-1::GFP::tubulin unc-119(+)]	This study
RL292	mes-1(bn7) IV; ruIs57[pie-1::GFP::tubulin unc-119(+)]	(Liro and Rose, 2016)
RL359	ced-10(t1875) dpy-20(e1282)/nT1[qIs51]	This study
RL393	ced-10(t1875) dpy-20(e1282)/ nT1 [qIs51(pha::GFP)] IV; ruIs57[pie-1::GFP::tubulin unc-119(+)]	This study
RL396	*par-2(it315[mCh::PAR-2])III;* ltIs37 [pie-1p::mCherry::his-58 + unc-119(+)] him-8(e1489) IV; ruIs57[pie-1::GFP::tubulin + unc-119(+)]	(Koch and Rose, 2023)
RL412	par-2(it315[mCh::PAR-2])III; unc-119(ed3) III; ced-10(t1875) dpy-20(e1282)/nT1[qIs51] IV; ruIs57[pie-1::GFP::tubulin unc-119(+)]; +/nT1[qIs51] V	This study
RL440	qyIs28 [ced-10p::GFP::ced-10; unc-119(+); unc-119(ed4); ced-10(t1875) dpy-20(?)/nT1[qIs51] IV; +/nT1[qIs51] V	This study
RL443	par-2(it315[mCherry::PAR-2 unc-119(+)]) III; unc-119(ed3) III; ruIs57[pie-1::GFP::tubulin unc-119(+)]	This study
TH246	unc-119(ed3) III; ddIs159[arx-2::TY1::EGFP::3xFLAG(92C12) + Cbr-unc-119(+)].	CGC; (Sarov et al., 2012)

493 RNA interference

494 For all target genes, RNAi was performed by feeding as described (Ahringer, 2006), with
495 the modification of adding IPTG to the bacterial culture, to a final concentration of 1mM, just
496 prior to seeding the culture on the feeding plates. Plates were then kept in the dark at 4°C for no
497 more than 5 days prior to use. The following RNAi feeding clones were obtained from the
498 Ahringer library (Kamath et al. 2003): arx-2 (V-7M13), mom-2 (V-6A13), mes-1(X-5L23); the
499 L4440 empty vector was used as control. For all conditions, worms were placed on plates seeded
500 with RNAi bacteria at the large L3 through L4 stages and grown at 20°C unless otherwise noted,
501 with imaging carried out at room temperature. For *arx-2*, worms were grown for 48-52hr; RNAi
502 was judged to be effective if many small cortical extrusions were present in early embryos and
503 there were unhatched siblings from same brood (Patel et al., 2008; Roh-Johnson and Goldstein,
504 2009). For *mom-2* RNAi in experiments to score spindle orientation, worms were grown for 36-
505 48h and RNAi was considered effective if *mes-1(bn7);GFP::tubulin; mom-2RNAi* embryos
506 filmed in parallel exhibited 80-100% abnormal spindle orientations; *mes-1* RNAi was carried out
507 for 24-20hr, and considered *effective if mom-5(zu193); GFP tubulin; mes-1(RNAi)*embryos
508 treated in parallel exhibited 80-100% abnormal spindle orientations as in (Liro and Rose, 2016).
509 For *mom-2* and *mes-1* RNAi used to assess P granules, worms were grown at 16 for 48-72 hours,
510 with RNAi effectiveness determined by enhancement of *mes-1(bn7)* or *mom-2(or42)*
511 respectively as above.

512 The *ced-10* RNAi clone obtained from our library (IV-1J04) was found to contain no
513 insert. An RNAi feeding construct was generated by subcloning the *ced-10* cDNA region of
514 pPR37 (constructed by Peter Reddien, courtesy of Erik Lundquist) into the NcoI and SacI sites of
515 the L4440 vector. The plasmid was transformed into HT115 and sequence confirmed. Defects in
516 P1 and EMS spindle rotation in *mom-5(zu193); GFP::tubulin; ced-10(RNAi)* embryos confirmed
517 that CED-10 knockdown with this plasmid was sufficient to induce an enhanced spindle
518 phenotype, after 48-52h feeding at 20°C. Many small cortical extrusions were also present in
519 these embryos, as reported for *ced-10(t1875)* (Price et al., 2022). In parallel experiments,
520 knockdown efficacy was assessed by quantifying the depletion of fluorescent protein in
521 GFP::CED-10; *ced-10(RNAi)* embryos after 48-52h at 20°C, which resulted in a reduction of the
522 GFP signal to background N2 levels as described in the text; however, older embryos still
523 showed CED-10::GFP. In addition, most *ced-10(RNAi)* embryos hatched, indicating that RNAi is

524 not as strong as the null allele, but resembles published viable hypomorphic alleles (Kinchen et
525 al., 2005; Lundquist et al., 2001). The following conditions were then used for RNAi of CED-10
526 for different experiments: For immunostaining for MES-1, 28-30hrs of feeding at room
527 temperature, with the appearance of cortical blebs as a readout of RNAi efficacy. For GFP::SRC-
528 1, ARX-2::GFP, and gut granule assays, feeding was carried out at 48-72 hours at 16C to allow
529 for longer production of embryos. In addition to scoring for cortical blebs, enhancement of either
530 the *mom-5* or *mom-2* spindle orientations defects was scored first as above, to ensure for RNAi
531 effectiveness.
532
533 Live epifluorecence microscopy
534 Embryos were removed from gravid hermaphrodites in 1x Egg Buffer, and mounted on
535 2% agarose pads under coverslips. For most experiments, embryos were observed on an
536 Olympus BX60 microscope equipped with PlanApo N 60X, 1.42 NA oil immersion objective
537 lens, a CoolLED light source, a Hamamatsu Orca 12-bit digital camera, and MicroManager
538 software (Hardin, 2011; Strange et al., 2007).
539 To score P1, EMS, and P2 spindle positioning, images were acquired every 10 s with an
540 exposure of 10 ms in bright field illumination. Focus was manually adjusted to follow
541 centrosomes during each division. In strains expressing GFP::tubulin (all but *mom-2(or42)*),
542 acquisition was switched to 488 nm light at approximately NEB of the ABa and ABp cells; this
543 allows a more precise following of centrosomes and spindles in the EMS cell in mutants, because
544 the centrosomes typically set up on the left-right axis in this cell. The same conditions were used
545 to visualize GFP;;tubulin (10ms, 488nm) and PAR-2::mCherry (200ms, 560nm) localization,
546 with the addition of fluorescence images at the start of the P1 cell cycle, at NEB/metaphase, and
547 at P1 cytokinesis to score the P1 PAR-2 domain. To visualize GFP::CED-10, single-plane
548 images were acquired with an exposure of 100 ms of 488nm light every 30 s.
549 For the *mom-2(or42)* single and double mutant experiments and gut granule experiments,
550 embryos were prepared as above and imaged on an Olympus BX53 microscope equipped with
551 PlanApo N 60X, 1.42 NA oil immersion lens, a Hamamatsu Orca Fusion BT camera, a SpectraX
552 light engine, and motorized turret, all run by Olympus Cellsens software.
553
554

555 Confocal microscopy

556 Embryos were removed from gravid hermaphrodites and mounted as above, and were
557 observed using the spinning disc module of an Intelligent Imaging Innovations (3i) Marianas
558 SDC Real-Time 3D Confocal-TIRF microscope fit with a Yokogawa spinning disc head, a 60x
559 1.4 numerical aperture oil-immersion objective, and EMCCD camera, at 100% 488 nm laser
560 power. Acquisition was controlled by Slidebook 6 software (3i Incorporated). To visualize
561 GFP::SRC-1, single-plane images were acquired with an exposure of 500 ms every 30 s. To
562 visualize ARX-2::GFP, Z-stack images were acquired with a total depth of 14 um and a step size
563 of 2 um at an exposure of 500 ms every 30 s.

564

565 Scoring asymmetric division

566 Nuclear rotation was scored by following centrosome movements in brightfield and/or
567 via tubulin fluorescence, with the angle of the nuclear-centrosome complex defined based on a
568 line drawn through the two centrosomes relative to a line drawn on the anterior-posterior axis of
569 the embryo. For the P1 cell, rotation was scored as "normal" if the nuclear-centrosome complex
570 rotated to within 30° of the anterior-posterior axis (= 0°) prior to NEB, late if after NEB but prior
571 to cytokinesis onset, and failed if rotation didn't occur. With either normal or late rotation, one
572 centrosome was also close to the AB/P1 cell contact after rotation. For the EMS cell, while in
573 many cells the centrosomes are initially on the left-right axis occurs, we observed some cases of
574 centrosome migration directly onto the anterior-posterior axis as previously reported (Liro and
575 Rose, 2016). Thus, nuclear centrosome orientation was scored as normal is the centrosome were
576 aligned with the anterior-posterior axis via either rotation or migration prior to NEB, and late if
577 orientation occurred via spindle movements after NEB; in both cases the posterior centrosome
578 was closer to the EMS/P2 contact at the end of an EMS division. A "failed" EMS rotation was
579 defined as a spindle that was oriented more than 45° off the anterior-posterior axis in any
580 direction at the end of division; the daughters cells in this case were in different focal planes after
581 division. For the P2 cell, control GFP::tubulin embryos were filmed to determine the time at
582 which close apposition of one centrosome to the EMS/P2 cell contact occurred, which can occur
583 through direct centrosome migration or a slight rotation of the nucleus. The nuclear-centrosome
584 complex and the subsequent spindle are thus oriented approximately 45° relative to the anterior-
585 posterior axis, a slightly dorsal/ventral orientation. This "centrosome cueing" occurred in all

586 control embryos, and the time ranged from 60sec before EMS NEB to 40 sec after in this data
587 set. Centrosome position was then scored as normal if centrosome cueing occurred within this
588 time range for GFP::tubulin strains.
589 Polarity was examined using mCh::PAR-2; GFP::tubulin expressing strains. For the P1
590 cell, embryos were scored as normal if a PAR-2 posterior domain was present by metaphase.
591 Embryos in which PAR-2 was inherited abnormally from the first division (e.g. laterally in both
592 AB and P1) were excluded from analysis, as the P1 cell would not be fated normally; this was
593 observed in 1/11 control embryos. For the P2 cell, a "normal" PAR-2 domain was restricted to
594 the ventral half to three-quarters of the cell; that is PAR-2 disappeared from at least the dorsal
595 half of the ABp contact and the dorsal-most aspect of the outer posterior membrane of P2, and
596 this occurred before P2 NEB. "Abnormal" P2 PAR-2 domains observed in both controls and
597 *ced-10* embryos included uniform presence of mCherry::PAR-2 on the entire surface of P2 and
598 the absence of mCherry::PAR-2 from the posterior cell surface only. P2 nuclear-centrosome
599 orientation in PAR-2 strains was scored as above, but we noted more variability in the time of P2
600 centrosome cueing in this strain, with some control embryos cueing as late as EMS NEB + 160
601 sec, and thus *ced-10* embryos were scored as normal if they exhibited cueing within this time
602 range.
603 To determine if embryos produced intestinal cells (an E cell derivative), embryos were
604 mounted on agar pads as outlined for imaging of early divisions above. After filming some
605 embryos to confirm spindle positioning phenotypes (e.g., in RNAi conditions), these and sibling
606 embryos on agar pads were incubated in a moist chamber at 16°C for 18-24 hr, until control
607 embryos had hatched. Polarization optics were then used to identify the presence of birefringent
608 gut granules, which are a marker of intestinal differentiation (Laufer et al., 1980).
609
610 <u>Analysis of cortical fluorescence intensity from live imaging</u>
611 Qualitative analysis of GFP::SRC-1 at the four-cell stage did not suggest any asymmetry
612 at the EMS/P2 contact; quantifications of the relative cortical fluorescence of EMS/P2 contact
613 compared to other contacts was measured from single images taken at the time of ABa/ABp
614 NEB (scored by the loss of exclusion of fluorescent signal from the nucleus), as this is within the
615 time period when published LIN-5 and Y99 asymmetries were visible. The "Segmented Line"
616 tool in ImageJ was used to trace a 3-pixel-wide line along the entire EMS/P2 contact and other

617 contacts, and the "Measure" function was used to obtain the mean fluorescence intensity of the
618 the line. The same line traces were placed approximately 5 -10 pixels from the cell-cell contacts,
619 avoiding the nucleus or centrosome, to sample mean cytoplasmic fluorescence intensity within
620 the adjacent cells. The fluorescence intensity of each cell-cell contact was then divided by the
621 mean cytoplasmic intensity of the two cells on either side of it to produce a relative cortical
622 fluorescence intensity. The EMS/P2 "Enrichment Index" was calculated as the ratio of
623 cytoplasm-normalized EMS/P2 contact fluorescence to the ratio of cytoplasm-normalized
624 EMS/ABp contact fluorescence for each embryo. A value of 1 indicates no difference in relative
625 cortical fluorescence intensity between the two cell-cell contacts, i.e., no enrichment.
626 For ARX-2::GFP, Maximum Z projections were generated for a timepoint 30-90 seconds
627 prior to EMS NEB, as this appeared qualitatively to be the time with the strongest cell contact
628 signal. Quantification of relative cortical intensity and enrichment were measured as above. For
629 CED-10::GFP epifluorescence images, measurements of relative cortical intensity and
630 enrichment were made on mid-focal plane images at ABa/ABp NEB as above, with the
631 modification that a 2-pixel segmented line was used. For the examination of CED-10::GFP
632 signal after RNAi of *ced-10*, the "freehand line" tool was used to trace around the embryo and
633 the mean fluorescence measured.
634
635 Immunostaining
636 Embryos were dissected in PBS from gravid hermaphrodites onto slides coated with
637 poly-L-lysine, then they were freeze-cracked in liquid N2 according to (Duerr, 2006) To stain
638 SRC-1 dependent phosphotyrosine as in (Bei et al., 2002), slides were immediately fixed in
639 prechilled methanol at -20°C for 5 min, followed by 5 min in ice-cold acetone, air-dried for 5-10
640 min at room temperature, and then rehydrated in PBS for 5 min. Slides were incubated in 50 uL
641 of blocking solution (5% w/v bovine serum albumin in PBS + 0.1% v/v Tween) in a moist
642 chamber for 2 hr at room temperature. After wicking excess blocking solution away, samples
643 were incubated in 50 uL of primary antibody solution (Santa Cruz Biotech mouse monoclonal
644 PY99 diluted 1:200 in PBS + 1% w/v bovine serum albumin + 0.1% v/v Tween, overnight in a
645 moist chamber at 4°C. Slides were washed 3x in PBS + 0.1% v/v Tween, then incubated in 50
646 uL secondary antibody solution (Alexa594-congugated goat monoclonal anti-mouse diluted
647 1:200 in PBS + 1% w/v bovine serum albumin + 0.1% v/v Tween) in a moist chamber for 2 hr at

room temperature. After washing 3x in PBS + 0.1% v/v Tween, slides were incubated in DAPI/PBS followed by one wash in PBS; excess PBS was wicked away and samples were preserved with 20 uL of Vectashield mounting medium with a 20 x 40 mm coverslip sealed with nail polish. To stain mNG::3xFLAG::MES-1, the same protocol was used, omitting the acetone fixation and air-drying steps. The primary antibody was Invitrogen mouse monoclonal anti-FLAG, diluted 1:500. Images of samples were acquired in the focal plane of the EMS/P2 contact with an exposure of 200 ms of 488 nm light and 10ms of UV LIGHT on the Olympus BX60 microscope described above. Quantification of cortical intensity and enrichment was carried out in ImageJ as described above for SRC-1::GFP. For mNG::3xFLAG::MES-1 staining, a Maximum Z projection of two mid focal plane images from each four-cell stage embryo was used. For Y99 staining, quantification was carried on single-plane images from embryos in prophase through early anaphase, as determined by DAPI staining.

References

Ahringer, J., 2006. Reverse genetics. WormBook.

Arata, Y., Lee, J.-Y., Goldstein, B., Sawa, H., 2010. Extracellular control of PAR protein localization during asymmetric cell division in the C. elegans embryo. Development, 3337-3345.

Bei, Y., Hogan, J., Berkowitz, L.A., Soto, M., Rocheleau, C.E., Pang, K.M., Collins, J., Mello, C.C., 2002. SRC-1 and Wnt signaling act together to specify endoderm and to control cleavage orientation in early C. elegans embryos. Developmental Cell, 113-125.

Bergstralh, D.T., St Johnston, D., 2014. Spindle orientation: what if it goes wrong? Semin Cell Dev Biol 34, 140-145.

Berkowitz, L.A., Strome, S., 2000. MES-1, a protein required for unequal divisions of the germline in early C. elegans embryos, resembles receptor tyrosine kinases and is localized to the boundary between the germline and gut cells. Development 127, 4419-4431.

Boreaux, A., Vignal, E., Faure, S., Fort, P., 2007. Evolution of the Rho Family of Ras-like GTPases in Eukaryotes. Molecular Biology and Evolution 24, 203-216.

Brenner, S., 1974. The genetics of Caenorhabditis elegans. Genetics 77, 71-94.

Bustelo, X.R., Sazeau, V., Berenjeno, I.M., 2007. GTP-binding proteins of the Rho/Rac family: regulation, effectors and functions in vivo. BioEssays 29, 356-370.

Cabello, J., Neukomm, L.J., Gunesdogan, U., Burkart, K., Charette, S.J., Lochnit, G., Hengartner, M.O., Schnabel, R., 2010. The Wnt pathway controls cell death engulfment, spindle orientation, and migration through CED-10/Rac. PLOS Biology, e1000297.

Chan, F.-Y., Silva, A.M., Saramago, J., Pereira-Sousa, J., Brighton, H.E., Pereira, M., Oegema, K., Gassman, R., Carvalho, A.X., 2018. The ARP2/3 complex prevents excessive formin activity during cytokinesis. Molecular Biology of the Cell 30, 96-107.

687 Church, D.L., Guan, K.L., Lambie, E.J., 1995. Three genes of the MAP kinase cascade, mek-2,
688 mpk-1/sur-1 and let-60 ras, are required for meiotic cell cycle progression in
689 Caenorhabditis elegans. Development 121, 2525-2535.
690 Cortes, D.B., McNally, K.L., Mains, P.E., McNally, F.J., 2015. The asymmetry of female
691 meiosis reduces the frequency of inheritance of unpaired chromosomes. Elife 4, e06056.
692 D'avino, P.P., Glover, D., Glover, D.M., 2005. Cleavage furrow formation and ingression during
693 animal cytokinesis: a microtubule legacy. Journal of Cell Science, 1549-1558.
694 di Pietro, F., Echard, A., Morin, X., 2016. Regulation of mitotic spindle orientation: an integrated
695 view. EMBO reports, 1106-1130.
696 Duerr, J.S., 2006. Immunohistochemistry. WormBook, 1-61.
697 Duquette, P.M., Lamache-Vane, N., 2014. Rho GTPases in embryonic development. Small
698 GTPases 5, 1-9.
699 Gillies, T.E., Cabernard, C., 2011. Cell Division Orientation in Animals. Current Biology 21,
700 R599-R609.
701 Griffin, E., 2015. Cytoplasmic localization and asymmetric division in the early embryo of
702 Caenorhabditis elegans. WIREs Dev Biol, 267-282.
703 Hall, A., 2012. Rho family GTPases. Biochemical Society Transactions 40, 1378-1383.
704 Hardin, J., 2011. Imaging Embryonic Morphogenesis in C. elegans, Methods in Cell Biology, pp.
705 377-412.
706 Heppert, J.K., Pani, A.M., Roberts, A.M., Dickinson, D.J., Goldstein, B., 2018. A CRISPR
707 tagging-based screen reveals localized players in Wnt-directed asymmetric cell division.
708 Genetics, 1147-1164.
709 Inaba, M., Yamashita, Y.M., 2012. Asymmetric Stem Cell Division: Precision for Robustness.
710 Cell Stem Cell, 461-469.
711 Kinchen, J.M., Cabello, J., Klingele, D., Wong, K., Feichtinger, R., Schnabel, H., Schnabel, R.,
712 Hengartner, M.O., 2005. Two pathways converge at CED-10 to mediate actin
713 rearrangement and corpse removal in C. elegans. Nature 434, 93-99.
714 Koch, L.A., Rose, L.S., 2023. Multiple pathways for reestablishing PAR polarity in C. elegans
715 embryo. Dev Biol 500, 40-54.
716 Kotak, S., 2019. Mechanisms of Spindle Positioning: Lessons from Worms and Mammalian
717 Cells. Biomolecules 9.
718 Laufer, J.S., Bazzicalupo, P., Wood, W.B., 1980. Segregation of developmental potential in early
719 embryos of Caenorhabditis elegans. Cell 19, 569-577.
720 Liro, M.L., Rose, L.S., 2016. Mitotic spindle positioning in the EMS cell of C. elegans requires
721 LET-99 and LIN-5/NuMA. Genetics, 1177-1189.
722 Lundquist, E.A., Reddien, P.W., Hartwieg, E., Horvitz, H.R., Bargmann, C.I., 2001. Three C.
723 elegans Rac proteins and several alternative Rac regulators control axon guidance, cell
724 migration and apoptotic cell phagocytosis. Development 128, 4475-4488.
725 Maduro, M.F., 2017. Gut development in C. elegans. Semin Cell Dev Biol 66, 3-11.
726 McNally, F.J., 2013. Mechanisms of spindle positioning. Journal of Cell Biology, 131-140.
727 Morin, X., Bellaiche, Y., 2011. Mitotic spindle orientation in asymmetric and symmetric cell
728 divisions during animal development. Developmental Cell, 102-119.
729 Ng, K., Hirani, N., Bland, T., Borrego-Pinto, J., Wagner, S., Kreysing, M., Goehring, N.W.,
730 2023. Cleavage furrow-directed cortical flows bias PAR polarization pathways to link cell
731 polarity to cell division. Curr Biol 33, 4298-4311 e4296.

732 Pacquelet, A., 2017. Asymmetric Cell Division in the One-Cell C. elegans Embryo: Multiple
733 Steps to Generate Cell Size Asymmetry. Results Probl Cell Differ 61, 115-140.
734 Patel, F.B., Bernadskaya, Y.Y., Chen, E., Jobanputra, A., Pooladi, Z., Freeman, K.L., Gally,
735 C.M., M. A., Soto, M.C., 2008. The WAVE/SCAR complex promotes polarized cell
736 movements and actin enrichment in epithelia during C. elegans embryogensis.
737 Developmental Biology 324, 297-309.
738 Price, K.L., Lamb, H., Alvarado, J.V., Rose, L.S., 2022. The DEPDC1 protein LET-99 is
739 required for cortical stability and antagonizes branched actin formation to promote robust
740 cytokinesis. bioRxiv.
741 Rocheleau, C.E., Downs, W.D., Lin, R., Wittmann, C., Bei, Y., Cha, Y.H., Ali, M., Priess, J.R.,
742 Mello, C.C., 1997. Wnt signaling and an APC-related gene specify endoderm in early C.
743 elegans embryos. Cell, 707-716.
744 Roh-Johnson, M., Goldstein, B., 2009. In vivo roles for Arp2/3 in cortical actin organization
745 during C. elegans gastrulation. J Cell Sci 122, 3983-3993.
746 Rose, L., Gonczy, P., 2014a. Polarity establishment, asymmetric division and segregation of fate
747 determinants in early C. elegans embryos. WormBook, 1-43.
748 Rose, L.S., Gonczy, P., 2014b. Polarity establishment, asymmetric division and segregation of
749 fate determinants in early C. elegans embryos. WormBook: The Online Review of C.
750 Elegans Biology.
751 Saenz-Narciso, B., Gomez-Orte, E., Zheleya, A., Gastaca, I., Cabello, J., 2016. Control of
752 developmental networks by Rac/Rho small GTPases: How cytoskeletal changes during
753 embryogenesis are orchestrated. Bioessays, 1246-1254.
754 Sarov, M., Murray, J.I., Schanze, K., Pozniakovski, A., Niu, W., Angermann, K., Hasse, S.,
755 Rupprecht, M., Vinis, E., Tinney, M., Preston, E., Zinke, A., Enst, S., Teichgraber, T.,
756 Janette, J., Reis, K., Janosch, S., Schoissnig, S., Ejsmont, R.K., Slightam, C., Xu, X., Kim,
757 S.K., Reinke, V., Stewart, A.F., Snyder, M., Waterson, R.H., Hyman, A.A., 2012. A
758 genome-scale resource for in vivo tag-based protein function exploration in C. elegans.
759 Cell 150, 855-866.
760 Sawa, H., 2012. Control of cell polarity and asymmetric division in C. elegans. Curr Top Dev
761 Biol 101, 55-76.
762 Sawa, M., Suetsugu, S., Sugimoto, A., Miki, H., Yamamoto, M., Takenawa, T., 2003. Essential
763 role of the C. elegans Arp2/3 complex in cell migration during ventral enclosure. Journal
764 of Cell Science, 1505-1518.
765 Schlesinger, A., Shelton, C.A., Maloof, J.N., Meneghini, M., Bowerman, B., 1999. Wnt pathway
766 components orient a mitotic spindle in the early Caenorhabditis elegans embryo without
767 requiring gene transcription in the responding cell. Genes & Development 13, 2028-2038.
768 Shakir, A.M., Jiang, K., Struckhoff, E.C., Demarco, R.S., Patel, F.B., Soto, M.C., Lundquist,
769 E.A., 2008. The Arp2/3 activators WAVE and WASP have distinct genetic interactions
770 with Rac GTPases in Caenorhabditis elegans axon guidance. Genetics 179, 1957-1971.
771 Stiernagle, T., 2006. Maintenance of C. elegans. WormBook, 1-11.
772 Strange, K., Christensen, M., Morrison, R., 2007. Primary culture of Caenorhabditis elegans
773 developing embryo cells for electrophysiological, cell biological and molecular studies.
774 Nature Protocols 2, 1003-1012.
775 Sugioka, K., Fielmich, L.-E., Mizumoto, K., Bowerman, B., van den Heuvel, S., Kimura, A.,
776 Sawa, H., 2017. Tumor suppressor APC is an attenuator of spindle-pulling forces during
777 C. elegans asymmetric cell division. Proc. Natl. Acad. Sci., 954-963.

Sugioka, K., Mizumoto, K., Sawa, H., 2011. Wnt regulates spindle asymmetry to generate asymmetric nuclear B-catenin in C. elegans. Cell 146, 942-954.

Sugioka, K., Sawa, H., 2010. Regulation of asymmetric positioning of nuclei by Wnt and Src signaling and its roles in POP-1/TCF nuclear asymmetry in Caenorhabditis elegans. Genes to Cells, 397-407.

Sumiyoshi, E., Takahashi, S., Obata, H., Sugimoto, A., Kohara, Y., 2011. The β-catenin HMP-2 functions downstream of Src in parallel with the Wnt pathway in early embryogenesis of C. elegans. Dev Biol 355, 302-312.

Thorpe, C.J., Schlesinger, A., Carter, J.C., Bowerman, B., 1997. Wnt signaling polarizes an early C. elegans blastomere to distinguish endoderm from mesoderm. Cell, 695-705.

Venkei, Z.G., Yamashita, Y.M., 2018. Emerging mechanisms of asymmetric stem cell division. Journal of Cell Biology, 3785-3795.

Walston, T., Tuskey, C., Edgar, L., Hawkins, N., Ellis, G., Bowerman, B., Wood, W., Hardin, J., 2004. Multiple Wnt signaling pathways converge to orient the mitotic spindle in early C. elegans embryos. Developmental Cell, 831-841.

Zhang, H., Skop, A.R., White, J.G., 2007. Src and Wnt signaling regulate dynactin accumulation to the P2-EMS cell border in C. elegans embryos. Journal of Cell Science, 155-161.

Zhu, Z., Chai, Y., Hu, H., Li, W., Li, W.-J., Dong, M.-Q., Wu, J.-W., Wang, Z.-X., Ou, G., 2020a. Spatial confinement of receptor activity by tyrosine phosphatase during directional cell migration. Proc. Natl. Acad. Sci. 117, 14270-14279.

Zhu, Z., Chai, Y., Hu, H., Li, W., Li, W.J., Dong, M.Q., Wu, J.W., Wang, Z.X., Ou, G., 2020b. Spatial confinement of receptor activity by tyrosine phosphatase during directional cell migration. Proc Natl Acad Sci U S A 117, 14270-14279.

Ziel, J.W., Hagedorn, E.J., Audhya, A., Sherwood, D.R., 2009. UNC-6 (netrin) orients the invasive membrane of the anchor cell in C. elegans. Nature Cell Biology 11, 183-189.